THE ASTROPHYSICAL JOURNAL, 473:864–872, 1996 December 20

TIME-DEPENDENT COOLING AND GRAIN DESTRUCTION IN HOT DUSTY PLASMAS: A SIMPLIFIED MODEL AND PRINCIPAL RESULTS

RANDALL K. SMITH,[1] LEO G. KRZEWINA,[2] AND DONALD P. COX
Department of Physics, University of Wisconsin – Madison, 1150 University Avenue, Madison, WI 53706
AND
RICHARD J. EDGAR[3] AND W. WARREN MILLER III
Department of Astronomy, University of Wisconsin – Madison, 475 N. Charter Street, Madison, WI 53706
Received 1993 April 26; accepted 1996 July 12

ABSTRACT

We present a simple method of including the principal effects of interstellar dust in hot gas evolution codes, including a consistent set of elemental abundances, their distribution among gas and grains in diffuse regions, the distribution of grain sizes, the sputtering of grains by impact with nuclei, and the cooling rate from gas-grain collisions. When combined with a gas evolution code, the time-dependent evolution of gas phase abundances, ion concentrations, and gas and grain cooling can be followed.

Sample calculations are presented to explore the relative timescales for grain destruction and radiative cooling, the relative importance of grain and gas cooling coefficients in evolving gas, the overall significance of grain inclusion to the thermal history of the gas, and the possibility of comparative dating of hot gas regions via their X-ray spectral characteristics.

We find that the straightforward comparison between the cooling coefficient of newly heated dust with that of gas in collisional equilibrium is particularly misleading. The cooling coefficient of newly heated material is overwhelmingly dominated by the nonequilibrium gas cooling, during which the ionization is rapidly rising and dust is being sputtered. The gas cooling coefficient drops rapidly during this brief period. Dust cooling also drops, because of the reduction in grain surface area. At high temperature, gas cooling soon falls below that of the grains, but grain cooling continues to fall rapidly, raising the gas cooling via the return of elements to the gas. For material whose temperature exceeds roughly 4×10^6 K, the total radiated energy during these "ion flash" and dust destruction epochs is small compared to the total energy in the system. Conversely, for temperatures below about 4×10^5 K, both grain destruction by ion sputtering and grain cooling are small. It is a somewhat remarkable coincidence: The range of temperature for which the dust destruction and radiative cooling timescales are comparable is also the temperature range for which grain and gas cooling rates are similar.

We conclude that the inclusion of dust in codes will usually have little overall effect on the thermal and dynamical history of the gas. But there can be a quite significant alteration of the X-ray spectra of recently heated gas, behind "nonradiative" shocks, for example. Dust inclusion at least at our level of complexity is required in any models purporting to examine spectral details. As an example, the inability of shockwave models to produce the surprising intensity of the [Fe x] line in the nonradiative shocks of the Cygnus Loop was once used to argue that the shock was proceeding through a medium infested with microscopic interstellar clouds, evaporating them as it went. It was suggested that evaporative injection of low ion stages into the hot gas could potentially produce the [Fe x], as iron is being ionized. Dust sputtering should produce a similar effect. There is probably an important spectral line whose intensity and surface brightness distribution map the pattern and rate of dust destruction in the Cygnus Loop and hot gas elsewhere, but it will not be found in gas-phase-only models. Fortunately, at the level of complexity of our modeling, dust inclusion is straightforward.

Subject headings: dust, extinction — ISM: general — plasmas

1. INTRODUCTION

Most models of cooling of hot interstellar plasmas have avoided the complications of the possible dust content of the gas, making the hopeful assumption that dust will be short-lived in such a hostile environment. That assumption, however, is rarely valid. Dust can be present for long periods of time and can cause modest changes in the evolution of hot gas and appreciably alter its observable characteristics. There have been many explorations of these important aspects of the dust/hot gas interaction, beginning perhaps with Ostriker & Silk (1973), who showed the importance of the dust cooling coefficient in high temperature gas. Examples of those who have explored both the cooling rate and dust sputtering include Burke & Silk (1974), Draine & Salpeter (1979), and McKee et al. (1987). Itoh (1989) explored the effect of dust sputtering on the ionization structure of X-ray emission of very high temperature shocks. Dwek (1981) considered the cooling and evolution of supernova remnants (SNRs) during the Sedov phase, and Vancura et al. (1994) explored in considerable

[1] Code 685, NASA Goddard Space Flight Center, Greenbelt, MD 20771.
[2] 801 Amanda Lane, Oldsmar, FL 34677.
[3] SAO, 60 Gardgen Street, MS70, Cambridge, MA 02138.

detail the structure and X-ray emission of steady state adiabatic shock waves.

The most important results of this effort have been that dust survives the shock transition, passing into the hot postshock environment, and that its radiation there is important and has been seen at the expected rate. Also important is that at temperatures below a few million K, dust is destroyed gradually over a very protracted period (owing to the broad distribution of grain sizes), and that except at rather low temperatures and in slow shocks the destruction takes place via thermal sputtering.

In this paper we describe the elementary approach we have taken toward incorporating these obviously important effects into hydrodynamic calculations of phenomena involving hot gas. Because of this focus we are able to make several simplifications. We are interested in dynamics in diffuse media and, in particular, gas that remains hot long after it is initially heated. We are not exploring the intimate details of any aspect of radiative shocks beyond the fact that the gas cools, or the distressing problem that dust destruction estimates significantly exceed those for its formation. As a result, we include only thermal sputtering by ions as a destruction mechanism and assume that on average, grains and gas are comoving coupled fluids. The recent paper by Vancura et al. (1994) provides an excellent example and reference set for the more complete description.

The codes that result from our study will be very useful for studying ancient hot gas bubbles as a possible model for the Local Bubble, fountains of hot gas rising out of the Galactic plane (or winds from the Galactic center), the hot interiors of individual old SNR bubbles in the Galactic plane and halo, models of superbubble evolution (for which much of the hot gas may have been heated by transport processes rather than by shocks), and many other large scale phenomena.

The basic information required for this project includes the following:

1. Total elemental abundances.
2. Fraction of each element found in grains in a diffuse interstellar environment.
3. Distributions of those elements among grain types.
4. Grain size distributions.
5. Mean grain densities (or porosity of grains).
6. Chemical inhomogeneities of the grains.
7. Rates of thermal sputtering by nuclei.
8. Rate of energy deposition in the grains due to electron impacts.

We discuss our assumptions about each of these and the reasons for ignoring other effects in § 2. In § 3 we present the method for incorporating this dust model into a code that calculates gas cooling rates. Finally, in § 4 we present representative single parcel evolutions (isothermal and isobaric) that follow the evolution of dust mass, cooling rate, and for the isobaric case, temperature. These results are very valuable in evaluating the importance of including dust in models of specific systems in which hot gas plays an important role.

As a final example, we present the effect that inclusion of dust has on the column densities of C IV, N V, O VI, Si IV, S IV, and S VI in one-dimensional isochoric and isobaric cooling flows, such as might exist in a galactic fountain. These results can be compared with the Edgar & Chevalier (1986) results calculated in a similar model without dust.

2. DUST PROPERTIES

Consultation with Mathis (1994) prompted us to include only the two most refractory components of interstellar dust, referred to as silicate grains and small carbon grains. We neglect grain mantles, which are not expected to be present in very diffuse interstellar conditions, and polycyclic aromatic hydrocarbons, which can easily be destroyed in the hot plasmas under consideration.

Our choices for the quantities of the various elements found initially in the gas phase, in the silicate dust, and in the carbon particles are shown in Table 1, both in the common logarithmic notation and in parts per million relative to hydrogen. The total abundances are taken from Anders & Grevesse (1989) and the depletions from Mathis (1992) and Spitzer & Jenkins (1975). In addition, we assume that the silicate dust consists of a homogeneous mixture of the elements within it.

The structure of silicate dust grains is not well known; recent evidence from cometary studies and X-ray halos around stars suggests that the mean internal density of dust grains might be quite low and, thus, that grains are fluffy or porous (Smirnov, Vaisberg, & Anisimov 1988; Mathis et al. 1995). However, there is no conclusive evidence, so all our calculations were done for both a solid, dense grain, and a porous, fluffy grain with one-fifth the density of the solid grain. We will occasionally refer to these by their respective

TABLE 1

DEPLETED GAS AND DUST CONSTITUENTS

	LOGARITHMIC[a]			PARTS PER MILLION H		
ELEMENT	Gas	Silicate	Carbon	Gas	Silicate	Carbon
Carbon	8.40	7.86	7.56	254	72	36
Nitrogen.....	8.05	...	...	112	0	0
Oxygen	8.83	8.26	...	673	180	0
Neon.....	8.09	...	...	123	0	0
Magnesium.....	6.11	7.57	...	1.3	37.1	0
Silicon	6.04	7.54	...	1.1	34.7	0
Sulfur	7.27	...	...	18.5	0	0
Argon.....	6.56	...	...	3.6	0	0
Calcium	2.60	6.34	...	4×10^{-4}	2.2	0
Iron	5.60	7.50	...	0.4	31.9	0
Nickel.....	4.00	6.25	...	1×10^{-2}	1.8	0
Aluminum	4.48	6.48	...	3×10^{-3}	3.0	0

[a] Where $H = 12.00$.

porosities, or empty volume fractions of 0 and 0.8, respectively. We use the following size distributions for silicate grains:

$$\frac{dN}{da} = Aa^{-p}, \quad <a < a_2, \tag{1}$$

where a is the grain radius. For the dense grains, $a_1 = 0.03$ μm, $a_2 = 0.23$ μm and $p = 3.5$, and for the fluffy grains, $a_1 = 0.03$ μm, $a_2 = 0.90$ μm and $p = 3.5$. This is the distribution given in Mathis & Whiffen (1987) with one modification, $p = 3.5$ instead of $p = 3.7$ for silicates, for reasons given later.

The mass in silicate or carbon grains per hydrogen atom is thus given by

$$M_g = \overline{\rho_g} \int_{a_1}^{a_2} \frac{4}{3} \pi a^3 \frac{dN}{da} da . \tag{2}$$

The normalization constant, A, was chosen such that the elemental abundances yield the chosen mean density for the grains. For the silicates, we have taken the density of solid grains to be $\bar{\rho}_g = 2.65$ g cm^{-3}, and that for porous grains to be $\bar{\rho}_g = 0.53$ g cm^{-3} (Mathis & Whiffen 1987).

For carbon grains, much less is known about the detailed size distribution, especially for small grain sizes. We used the distribution from Mathis, Rumpl, & Nordsieck (1977), with $p = 3.5$, $a_1 = 0.005$ μm, $a_2 = 1.0$ μm, and $\bar{\rho} = 2.0$ g cm^{-3}.

With the above choices, and the elemental abundances of Table 1, we find the grain size proportionality constant A, number per H atom, and mass per H atom shown in Table 2.

The sputtering of both silicates and small carbon grains by impacts with nuclei has been studied theoretically. We use the latest rates of Tielens et al. (1994), which are usefully quoted as polynomial fits to the function $\dot{a}(T)$, where $\dot{a} = da/dt$. Since the total sputtering yield is proportional to the density of the grain, $\dot{a}$ must be inversely proportional to the density, and we can scale these results for any grain density (Tielens et al. 1994).

In the temperature range of interest in this paper, cooling from dust grains arises primarily from deposition of energy by electron collisions with grains and by subsequent radiation in the infrared. The basic principle is that $nv/4$ impacts occur per unit area per second, bringing energy $m_e v^2/2$, for a total cooling rate per unit volume

$$\epsilon \sim n_e \left(\frac{m_e \langle v^3 \rangle}{8} \right) \left(\frac{S}{n_{\rm H}} \right) (n_{\rm H}) , \tag{3}$$

where S is the grain surface area per unit volume, and $S/n_{\rm H}$ is the grain surface area per hydrogen atom, given in our case by

$$\frac{S}{n_{\rm H}} = \int_{a_1}^{a_2} 4\pi a^2 \frac{dN}{da} da . \tag{4}$$

We have ignored the effects of grain charging, because the grain charge is thought to be negligible at temperatures above $\sim 2 \times 10^5$ K (McKee et al. 1987). Between 10^4 K and 2×10^5 K, the cross section for interactions with electrons would be considerably reduced by charges on the grains, which would significantly reduce dust cooling. However, the cooling due to dust is unimportant compared to that of the gas at such temperatures.

For constant grain properties, these considerations then give rise to a cooling coefficient

$$L_{\rm dust} = \frac{\epsilon}{n_e n_{\rm H}} \sim CT^{3/2} . \tag{5}$$

Early evaluations (e.g., Ostriker & Silk 1973) indicated that this cooling could exceed normal gas cooling for $T \geq 10^6$ K.

This simple picture, however, leads to serious overestimates of dust cooling. The most important additional requirements on a model are the following:

1. Using reduced grain surface area after some sputtering has occurred.
2. Taking into account the complete penetration of high speed electrons through very small grains, with a subsequent reduction in the energy deposition.

The first effect, the reduction of all grain surface areas and disappearance of the initially smaller grains requires only that size reduction be incorporated into the surface area integration. The second effect depends in detail upon the grain size and type and the electron energy. This was extensively studied in Dwek (1987), and Figures 3*a* and 3*b* of that paper present graphs of $h_e(a, T)$, the fractional efficiency in energy deposition due to electron penetration of the grains. We fitted the curves by an approximate formula:

$$h_e(a, T) = \frac{0.875a}{a + \beta(T)} , \tag{6}$$

where $\beta(T) = 0.01(T/T_c)^{1.75}(\rho_{\rm solid}/\rho)$ μm, with $T_c = 3.8 \times 10^6$ K for graphite dust and $T_c = 6 \times 10^6$ K for silicate dust. While not perfect, this formula fits the data well in general, overestimating the cooling for small grains and underestimating it for large grains. It is good to within 75% everywhere of interest, and usually much better, with the advantage of being easily calculated.

Thus, our formula for the cooling coefficient due to dust is

$$L_{\rm dust} = \frac{4\sqrt{2\pi}(kT)^{3/2}}{\sqrt{m_e}} \times \sum_i \left[A \int_{\max(a_1 - \delta, 0)}^{a_2 - \delta} \frac{a^2}{(a + \delta)^p} \frac{0.875a}{a + \beta(T)} da \right]_i , \tag{7}$$

where a is a grain's current radius, $a + \delta$ is its radius before sputtering has reduced each grain radius by $\delta = \int_{t_0}^{t} -\dot{a}\, dt$, and the sum is over the two types of grains. The coefficient in front is from the factor $m_e \langle v^3 \rangle/8$ in ϵ. In the general case with arbitrary p, this reduces to a hypergeometric function that is not convenient to evaluate except via tables. However, in the special case where p is an integer or half-integer, the integral can be solved analytically in a form easy to compute (Gradshteyn & Ryzhik 1980, pp. 75–79, 284, 1045). For $p = 3.5$, we get

$$\int \frac{a^3 da}{(a + \delta)^{7/2}(a + \beta)} = \frac{2\delta[15a^2(3\beta^2 - 3\beta\delta + \delta^2) + 5a(15\beta^2\delta - 13\beta\delta^2 + 4\delta^3)]}{15(\beta - \delta)^3(a + \delta)^{5/2}} + \frac{2\delta(33\beta^2\delta^2 - 26\beta\delta^3 + 8\delta^4)}{15(\beta - \delta)^3(a + \delta)^{5/2}} + K(a, \beta, \delta) , \tag{8}$$

TABLE 2

DUST PARAMETERS

Grain Type	A (μm^{p-1} grains per H atom)	N (grains per H atom)	M_g (grains per H atom)
Dense silicates.....	1.9×10^{-15}	4.8×10^{-12}	1.3×10^{-26}
Fluffy silicates.....	3.7×10^{-15}	9.5×10^{-12}	1.3×10^{-26}
Graphite	4.6×10^{-17}	1.0×10^{-11}	7.2×10^{-28}

where $K(a, \beta, \delta)$ depends upon the value of $\beta - \delta$:

$$K(a, \beta, \delta) = \frac{2\beta^3}{(\beta - \delta)^{7/2}} \arctan\left(\sqrt{\frac{a+\delta}{\beta - \delta}}\right), \quad \beta - \delta > 0 , \tag{9}$$

$$K(a, \beta, \delta) = \frac{2\beta^3}{(\delta - \beta)^{7/2}} \operatorname{arctanh}\left(\sqrt{\frac{a+\delta}{\delta - \beta}}\right), \quad \beta - \delta < 0 . \tag{10}$$

However, in the special case where $0.95\delta < \beta < \delta$ the above solution is numerically problematic. In this case, it is possible to do an expansion on the small term $\gamma = \delta - \beta$, resulting in the expression

$$\int \frac{a^3 da}{(a+\delta)^{7/2}(a+\delta-\gamma)} = \int \frac{a^3 da}{(a+\delta)^{9/2}} + \gamma \int \frac{a^3 da}{(a+\delta)^{11/2}} . \tag{11}$$

To verify the final result, in Figure 1 we compare the equilibrium gas and initial dust cooling coefficients versus temperature with the result given in Dwek (1987). Gas cooling is shown for the Raymond & Smith (1977, 1993) code, both for depleted and solar abundances. In agreement with Ostriker & Silk (1973), Figure 1 demonstrates that the cooling of pristine dust is much larger than the equilibrium gas cooling at high temperatures. As we shall see, however, this comparison can be quite misleading.

3. USE WITH GAS EVOLUTION PROGRAMS

A common example of the use of gas evolution codes is in connection with a hydrodynamic simulation with a Lagrangian mesh, following the evolution of the location and state of a set of interacting gas parcels. The hydrodynamic code evaluates velocities, locations, densities, and temperatures, but requires the cooling coefficients for the gas parcels at each time step. The gas code uses ionization, recombination, and excitation rates to follow ion concentration evolution and to provide the cooling coefficients. It is accessed separately for each parcel at each time step, with the current ion concentrations, density, and temperature. It returns the new ion concentrations and the present gas cooling coefficient.

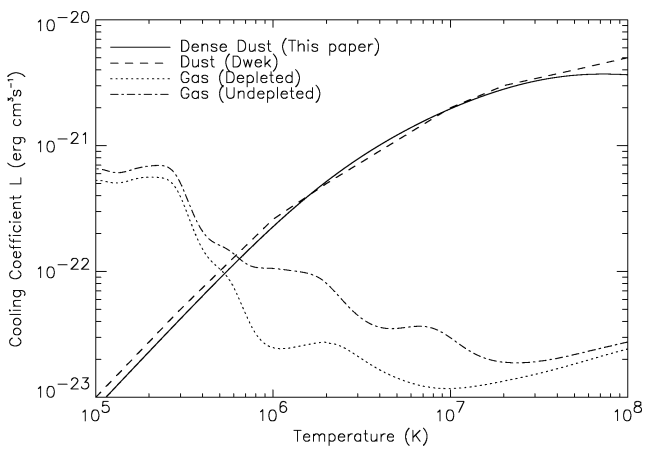

FIG. 1.—Collisional equilibrium gas and initial (dense) dust cooling coefficients vs. temperature.

When a dust code is grafted into this arrangement, the gas phase abundances become variables. In addition, one must store for each parcel two more variables describing the current state of grain destruction (one for each grain type). Thus, the grain code is accessed for each parcel with the current gas phase abundances, ion concentrations, two-grain destruction parameters, density, temperature, and time step. It calculates the mass returned to the gas during the time step, the new gas phase abundances, renormalized ion concentrations (assuming freshly sputtered material is neutral), and the grain cooling coefficient. The main program then sums the gas and grain cooling coefficients and continues. In models that decouple the gas and grain motions (e.g., Vancura et al. 1994) much more elaborate bookkeeping is required.

When snapshots of the structure are desired, one must save for each parcel the current gas phase elemental abundances in addition to the usual ion concentrations, density, temperature, location, velocity, and so on to be able to compute ion density distributions, column densities, line profiles, and emission spectra.

4. SINGLE PARCEL EVOLUTIONS

4.1. *Isothermal Evolution*

Starting with a parcel of gas at equilibrium ion concentrations appropriate to $T_0 = 2 \times 10^4$ K (so that hydrogen is fully ionized), we raise the temperature suddenly to a constant high value T_h. The gas scrambles upward in ionization state, the gas cooling coefficient drops rapidly as the lower stage ions disappear, and the dust gradually sputters, lowering the dust cooling coefficient but raising the gas phase abundances.

For single parcel evolutions, the heating, cooling, ionization, and recombination rates are all proportional to the electron density n_e. As a consequence, evolution depends only on the composite variable fluence:

$$f \equiv \int n_e \, dt . \tag{12}$$

Figure 2 shows the contours of dust mass fraction remaining as a function of fluence and T_h for dense silicate dust; graphite is not included due to its small mass contribution. One of the principal features of this result is that

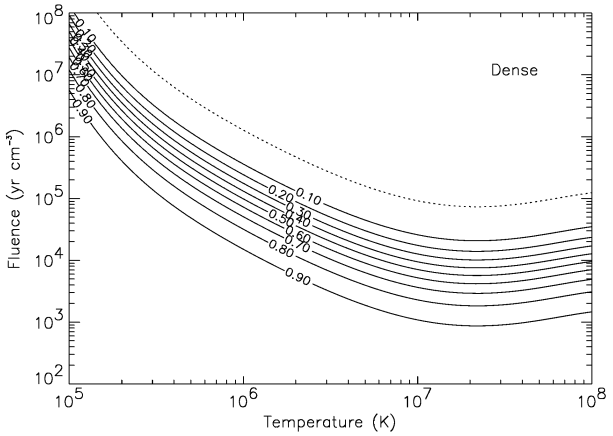

FIG. 2.—Dense silicate dust mass fraction remaining vs. fluence in an isothermal evolution, vs. temperature. Dotted line indicates completion of dust sputtering.

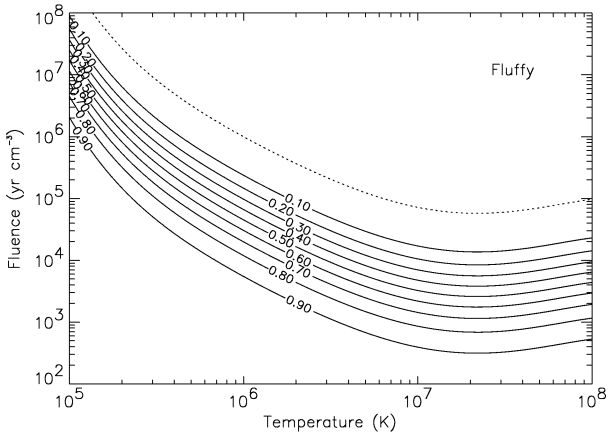

FIG. 3.—Same as Fig. 2 for fluffy dust

dust sputtering on the assumed grain size distribution is a very protracted process. It demonstrates, for example, that at a temperature of 10^6 K and electron density of 5×10^{-3} cm^{-3} (parameters typical in Local Bubble models), complete sputtering of dense silicate dust takes $\sim 3 \times 10^8$ yr, far longer than any age estimate for the Local Bubble, while dust is 10% and 50% sputtered at 3×10^6 and 2×10^7 yr, respectively. At a given grain size our fluffy dust (Fig. 3) is sputtered 5 times faster, but because the maximum grain size is 3.9 times larger, total destruction is only about 20% faster.

Figure 4 shows the evolution of the cooling coefficient and dust mass with fluence, for gas with graphite and dense silicate grains initially shocked from $T_0 = 2 \times 10^4$ to $T_h = 10^6$ K and then held at that temperature. Figure 5 is the same but for fluffy silicate grains. The cooling from gas (principally line emission) and from dust are shown along with the total. The dust mass evolution again illustrates the protraction of the sputtering process. The cooling graphs show that dust is an important coolant before the numerous tiny grains are destroyed, but a significant amount of dust mass is present long after its cooling contribution has become negligible.

4.2. *Isobaric Evolutions*

In our isobaric (constant pressure) conditions, gas is suddenly heated from equilibrium ionization at $T_0 = 2 \times 10^4$ K and then allowed to cool according to

$$\frac{dT}{df} = \frac{1}{n_e}\frac{dT}{dt} = -\frac{2}{5}\frac{L}{\chi k_B}\frac{1}{1.1}, \tag{13}$$

where $Ln_e n_H = Ln_e n/1.1$ is the volume emissivity, $p = \chi n k_B T$ is the pressure, $\chi = (n + n_e)/n$ is the number of free particles per nucleus, and k_B is the Boltzmann constant. (We have assumed $n = n_H + n_{He} = 1.1 n_H$, which for fully ionized gas yields $\chi = 2.3/1.1$.)

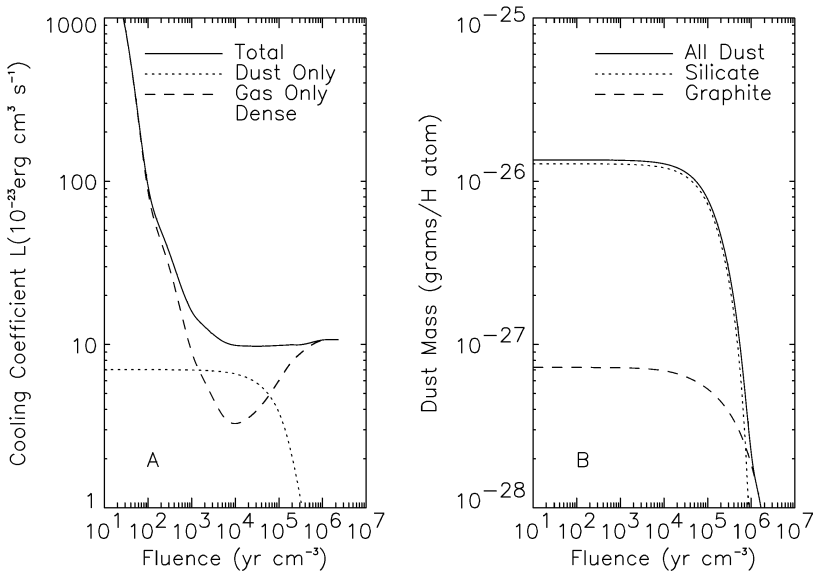

FIG. 4.—Evolution of cooling coefficient (*a*) and dust mass (*b*) for isothermal model at 10^6 K with dense dust. Initial condition was ionization equilibrium at 2×10^4 K.

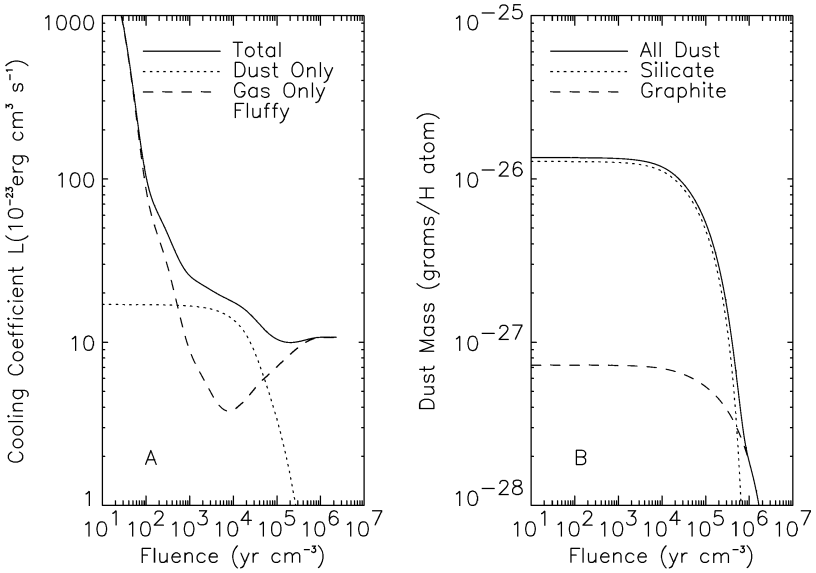

FIG. 5.—Same as Fig. 4 for fluffy dust

With these conditions, the cooling coefficient is initially large due to the presence of neutrals and low stage ions, but decreases rapidly as they ionize to higher stages. If T_h is very high, dust cooling is important after the initial "ion flash," but as the temperature drops, ion cooling again becomes dominant. Dust sputtering returns mass to the gas phase, but unless the initial temperature was above a critical value, sputtering is incomplete.

Figure 6 shows the isobaric evolution of the cooling coefficient and temperature for $T_h = 10^6$ K, comparing runs with and without dust (the latter starting with all material in the gas phase), for both silicate porosities.

Figure 7 shows the value of the fluence, f_{cool}, at which the temperature drops to 10^4 K, for isobaric runs both with dust of both porosities and without dust. Also shown is the fluence at which the dense and fluffy dust grains are completely sputtered in isothermal evolutions.

Figure 8 shows the dust mass fraction remaining in the gas when it finishes cooling, as a function of temperature T_h, for isobaric runs with both fluffy and dense grains.

Figures 9 and 10 show evolution of the cooling coefficient with temperature for runs beginning at $T_h = 10^6$ and 10^7 K. Results are shown for isobaric evolutions without dust and with dust of each grain type.

Figure 11 shows one spectral consequence of (dense) dust sputtering by comparing the strengths of two emission lines in the soft X-ray regime. For gas with unsputtered dust, i.e., with depleted abundances, the S VIII 63.5 Å line dominates

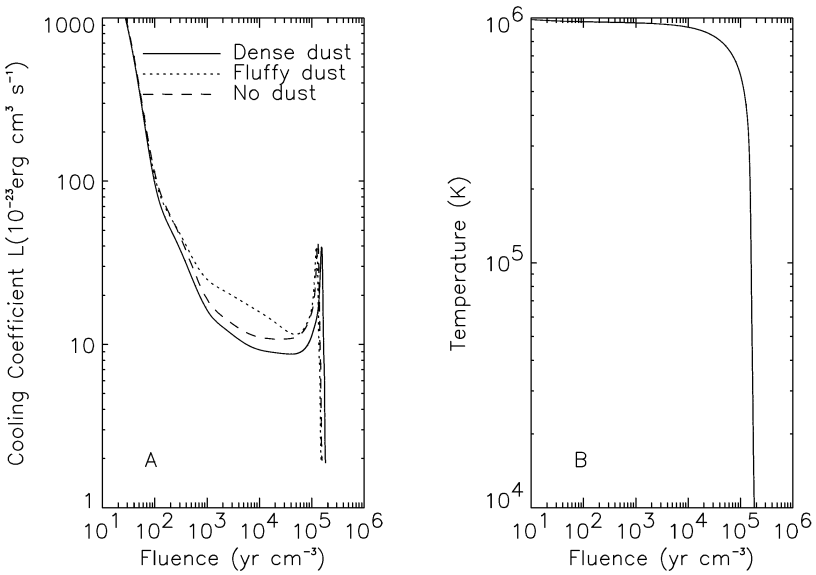

FIG. 6.—Evolution of cooling coefficient (*a*) and temperature (*b*) for isobaric models. Initial condition was ionization equilibrium at 2×10^4 K and kinetic temperature of 10^6 K.

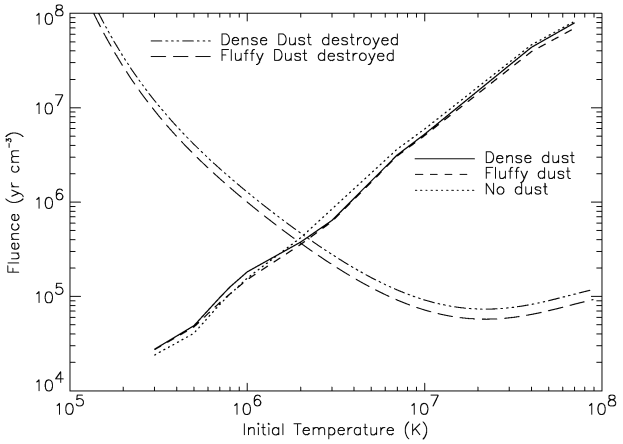

FIG. 7.—Fluence required in isobaric evolution to cool to 10^4 K vs. initial temperature. Also shown are the fluences at which dust would be fully destroyed at the initial temperature, from Figs. 2 and 3. Comparison shows the rapid switch in relative importance of dust destruction and radiative cooling for gas at different temperatures.

the 1/4-keV X-ray emission spectrum. However, for $f \gtrsim 10^5$ cm^{-3} yr, Si VIII 61.03 Å is stronger. Thus, the degree of sputtering in hot gas can potentially be measured by observing the soft X-ray spectrum.

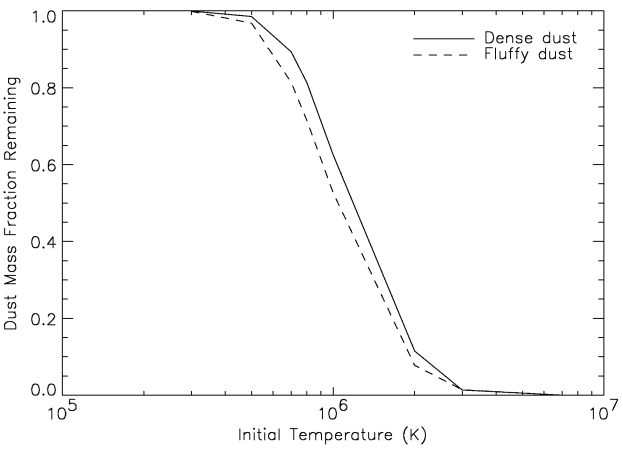

FIG. 8.—Dust mass fraction remaining after isobaric cooling to 10^4 K vs. initial temperature.

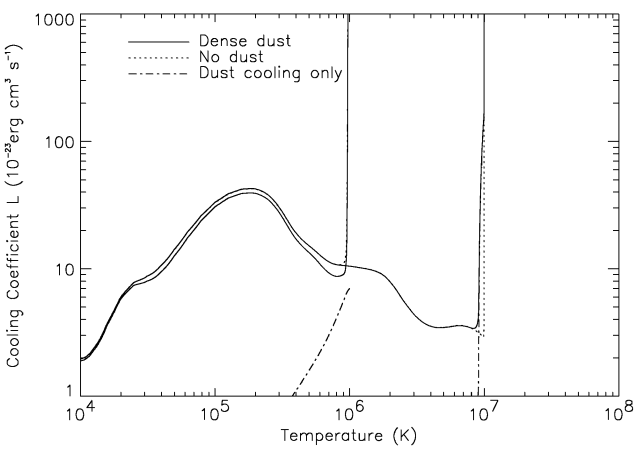

FIG. 9.—Cooling coefficient evolutions for isobaric cooling, starting from kinetic temperatures of 10^6 and 10^7 K and ionization equilibrium at 2×10^4 K. Huge ion flash and dust cooling epoch can easily be distinguished. Dense dust is used.

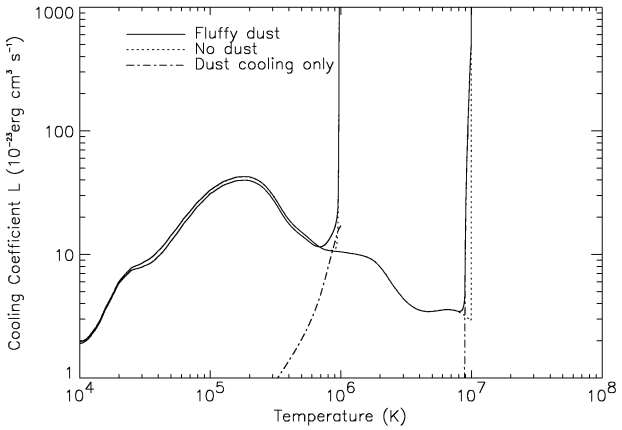

FIG. 10.—Same as Fig. 9 but with fluffy dust

5. FOUNTAIN COLUMN DENSITIES

We extended the calculations of Edgar & Chevalier (1986) to include the effects of dust depleting the available ions in the cooling fountain model they described, using an initial temperature of 10^6 K. We present in Table 3 the column densities of some astrophysically important ions that can be observed in the ultraviolet: C IV, N V, O VI, Si IV, S IV, and S VI. Four different models were considered: isobaric, isochoric, and two "transition" models that begin isobaric and switch to isochoric at either $T_{tr} = 2.2 \times 10^5$ K or $T_{tr} = 4.7 \times 10^5$ K. These same cases were considered by Edgar & Chevalier (1986). There are some differences between our dust-free results in Table 3 and those of Edgar & Chevalier (1986), mostly due to different choices of solar abundances. When using the same abundances, we find good agreement.

For an initial temperature of 10^6 K, dust destruction is incomplete in the fountain, lowering the column densities of carbon and silicon ions. Because the cooling of the gas is slightly slower with these depletions, the column densities of less depleted elements' ions are slightly enhanced.

6. DISCUSSION

From the results presented in Figures 2–11, a number of general conclusions can be drawn. From Figures 2 and 3,

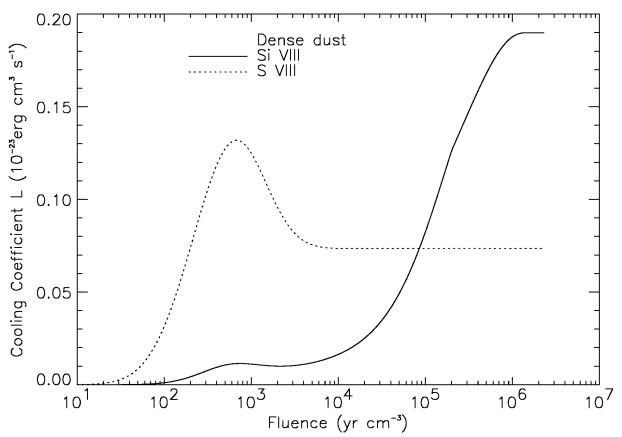

FIG. 11.—Spectral line cooling of Si VIII λ61 and S VIII λ63.5 vs. fluence at 10^6 K starting from ionization equilibrium at 2×10^4 K, with dense dust. The ratio of these two lines serves as a rough measure of the time since heating of the gas.

TABLE 3

FOUNTAIN COLUMN DENSITIES (cm^{-2})[a]

Dust	Model	C IV	N V	O VI	Si IV	S IV	S VI
None	Isochoric	9.3(13)	4.6(13)	6.9(14)	5.2(12)	1.2(13)	6.2(12)
None	$T_{tr} = 4.7 \times 10^5$ K	3.5(13)	2.1(13)	4.3(14)	1.9(12)	4.8(12)	3.3(12)
None	$T_{tr} = 2.2 \times 10^5$ K	1.9(13)	1.8(13)	4.6(14)	9.3(11)	2.3(12)	3.2(12)
None	Isobaric	1.2(13)	1.7(13)	4.6(14)	3.5(11)	1.4(12)	3.1(12)
Dense.....	Isochoric	7.5(13)	4.9(13)	6.6(14)	1.7(12)	1.3(13)	6.7(12)
Dense.....	$T_{tr} = 4.7 \times 10^5$ K	3.0(13)	2.3(13)	4.3(14)	8.5(11)	5.2(12)	3.7(12)
Dense.....	$T_{tr} = 2.2 \times 10^5$ K	1.7(13)	2.0(13)	4.6(14)	4.2(11)	2.5(12)	3.6(12)
Dense.....	Isobaric	1.1(13)	1.9(13)	4.6(14)	1.7(11)	1.6(12)	3.6(12)
Fluffy.....	Isochoric	7.5(13)	4.7(13)	6.2(14)	2.1(12)	1.3(13)	6.2(12)
Fluffy.....	$T_{tr} = 4.7 \times 10^5$ K	2.9(13)	2.1(13)	3.9(14)	9.6(11)	5.2(12)	3.4(12)
Fluffy.....	$T_{tr} = 2.2 \times 10^5$ K	1.6(13)	1.8(13)	4.2(14)	4.8(11)	2.5(12)	3.3(12)
Fluffy.....	Isobaric	1.0(13)	1.8(13)	4.2(14)	1.9(11)	1.6(12)	3.2(12)

[a] The numbers in parentheses are powers of 10.

one finds that the timescale for complete sputtering of dust is long compared to other timescales of interest, even for fluffy dust. Between $T = 3 \times 10^5$ K and 4×10^7 K, at a typical interstellar pressure of $p/k = \chi nT = 10^4$ cm^{-3} K, the complete sputtering timescale of fluffy dust is approximately constant at 2.5×10^8 yr (within a factor of 2). It is even longer for lower or higher temperatures. As we pointed out previously, this is much longer than most estimates of the age of the Local Bubble. In the diffuse hot portions of the Cygnus Loop, the pressure is a factor of 100 higher. The corresponding sputtering time is only 3×10^6 yr, but even that is about a factor of 200 longer than the age of the remnant. Infrared emission from hot dust behind the adiabatic (X-ray emitting) shocks has been found and shown to be consistent with the dust survival predicted by models similar to ours (Arendt et al. 1992).

Such numbers must be considered cautiously, however. From Figures 2, 3, 4, and 5 it is clear that essentially all of the dust mass has been returned to the gas long before the largest grains are completely gone. For a heavily depleted element such as iron, even a few percent of mass return has a very large effect on the gas phase abundance and spectrum. In the Local Bubble (age 10^5 to perhaps 10^7 yr), a non-negligible amount of sputtering may have occurred.

From Figures 7 and 8, we find that at $T \gtrsim 4 \times 10^6$ K, complete dust sputtering occurs prior to substantial radiative cooling of the gas. We conclude that, for those temperatures at which pristine dust would dominate the total cooling rate, it cannot survive long enough for its radiation to alter the thermal history very much. Conversely, for temperatures between 10^4 and 3×10^5 K, both thermal dust sputtering and dust cooling are small. So if thermal sputtering is the only important destruction mechanism, gas in this temperature range will evolve with fixed (but depleted) elemental abundances, and be dominated by gaseous processes.

Again, these conclusions must be considered with caveats. Quite often, very high temperature gas cools at a much higher rate than that determined by its radiative emissivity, through adiabatic expansion (e.g., in the Sedov blast wave), or via thermal conduction to cooler material, or both. As a consequence, such gas will often not complete its sputtering before reaching lower temperatures at which the grains can survive (see also Dwek 1981). During this evolution, the grains can provide a large fraction of the emission, though they do not radiate a significant fraction of the total energy available. Similarly, gas below 3×10^5 K has often been much hotter in the past and can have had a significant amount of dust sputtering. Clearly, the history of a gas parcel must be considered carefully when an estimate is made of its dust content or gaseous abundances (Dwek 1981).

Many aspects of the cooling behavior of shock-heated material are evident in Figures 4–6. At 10^6 K, the initial dust cooling coefficient is comparable to the equilibrium gas cooling coefficient, higher for fluffy dust and lower for dense. However, at early times, cooling is dominated by the gas in a brief "ion flash." The latter is due to the initial presence of low stages of ionization radiating profusely in the hot gas. As the ionization level scrambles upward toward equilibrium, the flash dies out, in this case after a fluence of about 1000 cm^{-3} yr. For a time thereafter, dust is an important coolant. It decreases due to sputtering at fluences $\gtrsim 3 \times 10^4$ cm^{-3} yr. The evolutions of isothermal and isobaric cases are nearly identical for fluence less than about 3×10^4 cm^{-3} yr, since the total temperature change is quite small. Finally, the isobaric case begins to cool significantly and passes through temperatures at which the cooling function is large (see Figs. 6, 9, and 10). The isothermal case has a gradually increasing gaseous cooling coefficient as continued sputtering completes the mass return. Its final plateau is the equilibrium cooling coefficient at 10^6 K for undepleted abundances.

The temperature of 10^6 K is in the most complex regime, where cooling and dust sputtering have similar timescales, and (coincidentally) grain and gas cooling coefficients are similar in magnitude. During its history the gas experiences radically different cooling coefficients. The gas and grain cooling contributions are so similar that in Figure 6 the total cooling rate curves for the two dust types straddle the curve for the dust-free evolution.

Despite this, some simplifying approximations to the cooling coefficient are possible, as the nearly straight lines of the cooling fluences in Figure 7 suggest. Supposing for the moment that the cooling coefficient at each temperature were a well-defined function, $L(T)$, the cooling fluence for isobaric evolution would be

$$f_{\rm cool}(T_h) = \frac{5}{2}\,\chi k_{\rm B} \int_{T_0}^{T_h} \frac{dT}{L(T)}\,, \qquad (14)$$

while for isochoric evolution the 5/2 is replaced by 3/2. Apart from very minor wiggles (due to real features in the cooling curve), the cooling fluences in Figure 7 are well fit

by a $T^{3/2}$ proportionality. Such a relationship has long been used to approximate the cooling; it is originally due to Kahn (1975, 1976), and the corresponding cooling coefficient, $L(T) \approx \alpha T^{-1/2}$ is called the Kahn approximation. The effective value of α generally used is 1.3×10^{-19} cgs (e.g., Cui & Cox 1992, and references therein), but 1.0×10^{-19} cgs is a better fit to the cooling fluences in Figure 7 and the cooling function itself (Figs. 9 and 10) for $T > 4 \times 10^5$ K and is used in equation (15).

The Kahn approximation has the useful feature that the cooling timescale from initial conditions T_h, n_h

$$t_{\rm Kahn}(T_h, n_h) = \frac{\chi k_{\rm B}}{\alpha n_h} T_h^{3/2} = 0.9 \times 10^5 \text{ yr} \left(\frac{T_h}{10^6 \text{ K}}\right)^{3/2} \left(\frac{\text{cm}^{-3}}{n_h}\right) \quad (15)$$

is independent of the subsequent thermal and pressure history of the gas. The fact that this relationship is apparently reliable over the entire range of T_h from 3×10^5 to 10^8 K, independent of the initial dust content of the gas, will be extremely useful for approximate modeling.

Figures 9 and 10 show the time-dependent cooling coefficient versus the time-dependent temperature, for isobaric cases with and without dust and for $T_h = 10^6$ and 10^7 K. Several features are noteworthy. Both the ion flash and the dust destruction epoch are very short at $T_h = 10^7$ K, but in the $T_h = 10^6$ K case the dust is never fully destroyed. At lower temperatures, the dust contribution to cooling is negligible, so with dust the $T_h = 10^6$ K cooling curve is slightly lower than the other cases, due to its depleted abundances.

If the eight curves of Figures 9 and 10 are superimposed (rather than two sets of four as shown), one finds that the postflash evolutions are nearly identical. There is little dependence on initial dust content of the gas (solid lines vs. dotted lines), or on initial temperature. The latter effect was previously noted by Edgar & Chevalier (1986). The differences between the various curves below 10^6 K are due almost solely to the different final gas phase abundances. In the fluffy grains, $T_h = 10^7$ K case, nearly all the dust is returned to the gas phase well before the temperature reaches 10^6 K. However, in the dense grains, $T_h = 10^6$ K run, there is a pronounced dip in the cooling curve, due to the dust that is no longer cooling effectively by itself but is still locking up important coolants.

Finally, Figure 11 shows an example of the sensitivity of the spectrum of hot gas to the effects of nonequilibrium ionization and dust content. The model starts with gas and dust at $T = 2 \times 10^4$ K and then makes a jump to $T = 10^6$ K, after which the system is isothermal. At 10^6 K, both the 61.0 Å line of Si VIII and the 63.5 Å line of S VIII are important emitters. The figure shows how the strengths of these two lines vary with fluence, while the temperature is held constant. Initially, the gas is singly ionized, but after a fluence of about 6500 cm^{-3} yr, the relevant ion populations approach equilibrium. In our model, none of the sulfur is in the dust, but at first 97% of the silicon is. The rise and then small decrease in the sulfur line strength is due to the scrambling of the gas through the S VIII ionization state until it reaches equilibrium. During the subsequent period (fluence $\gtrsim 3 \times 10^4$ cm^{-3} yr), the silicon line strength increases dramatically, as silicon returns to the gas phase.

The above results offer a method of approximate dating of hot gas with good X-ray spectral information, though it must generally be applied within the context of a specific model. The age of hot gas, i.e., the time since heating, can be inferred from the dust-sensitive spectral features, given separate information on the density and temperature structures and a scenario for the past history. In addition, because of the uncertainties of dust properties, the sputtering rate will not be absolutely calibrated. Still, it will be an extremely useful tool in helping to select among models for the approximately useful subset.

We have suggested that inclusion of dust evolution and cooling in hydro codes has both a small effect on the thermal evolution and large effects on observables. We can offer a better idea of the importance to the thermal evolution. In our isobaric evolutions with $T_h \gtrsim 10^6$ K, the total energy radiated by dust during the entire cooling evolution was approximately 100 eV $(T_h/10^6 \text{ K})^{1/2}$ per hydrogen atom, out of a total enthalpy of 500 eV $(T_h/10^6 \text{ K})$. The fraction of energy radiated by dust peaks in the vicinity of 10^6 K, at about 20%, dropping sharply at lower temperatures. Thus, these losses are never as significant as the uncertainties in the gas cooling coefficient itself. Nevertheless, some caution is required in their interpretation. For example, in a Sedov SNR evolution, the energy is effectively reused to heat more and more gas to ever lower temperatures. It is easily possible that as much as 30% of the total explosion energy is radiated by dust prior to the shell formation epoch (Dwek 1981).

The authors acknowledge useful discussions with John Mathis and Eli Dwek. This work was supported by NASA grants NAGW-2532, NAG5-629, and NAG5-3155, and one of the authors (R. K. S.) was supported on NSF and WARF Fellowships. L. G. K. acknowledges support from an Undergraduate Hilldale Fellowship from the University of Wisconsin–Madison.

REFERENCES

Anders, E., & Grevesse, N. 1989, Geochim. Cosmochim. Acta, 53, 197
Arendt, R. G., Dwek, E., & Leisawitz, D. 1992, ApJ, 400, 562
Burke, J. R., & Silk, J. 1974, ApJ, 190, 1
Cui, W., & Cox, D. P. 1992, ApJ, 401, 206
Draine, B. T., & Salpeter, E. E. 1979, ApJ, 231, 438
Dwek, E. 1981, ApJ, 247, 614
———. 1987, ApJ, 322, 812
Edgar, R. J., & Chevalier, R. A. 1986, ApJ, 310, L27
Gradshteyn, I. S., & Ryzhik, I. M. 1980, Table of Integrals, Series, and Products (4th. ed.; New York: Academic Press)
Kahn, F. D. 1975, Proc. 15th Int. Cosmic-Ray Conf. (Munich), 11, 3566
———. 1976, A&A, 50, 145
Itoh, H. 1989, PASJ, 41, 853
Mathis, J. S. 1992, private communication
———. 1994, private communication
Mathis, J. S., Cohen, D., Finley, J. P., & Krautter, J. 1995, ApJ, 449, 320
Mathis, J. S., Rumpl, W., & Nordsieck, K. H. 1977, ApJ, 217, 425
Mathis, J. S., & Whiffen, G. 1989, ApJ, 341, 808
McKee, C. F., Hollenbach, D. J., Seab, C. G., & Tielens, A. G. G. M. 1987, ApJ, 318, 674
Ostriker, J., & Silk, J. 1973, ApJ, 184, L113
Raymond, J. C., & Smith, B. W. 1977, ApJS, 35, 419
———. 1993, private communication
Smirnov, V. N., Vaisberg, O. L., & Anisimov, S. 1988, A&A, 187, 774
Spitzer, L., Jr., & Jenkins, E. B. 1975, ARA&A, 13, 133
Tielens, A. G. G. M., McKee C. F., Seab, C. G., & Hollenbach, D. J. 1994, ApJ, 431, 321
Vancura, O., Raymond, J. C., Dwek, E., Blair, W. P., Long, K. S., & Foster, S. 1994, ApJ, 431, 188